Hindawi Publishing Corporation
International Journal of Nuclear Energy
Volume 2014, Article ID 402351, 17 pages
http://dx.doi.org/10.1155/2014/402351

Research Article

Thermal Analysis of ZPPR High Pu Content Stored Fuel

Charles W. Solbrig, Chad L. Pope, and Jason P. Andrus

Idaho National Laboratory, Idaho Falls, ID 83404, USA

Correspondence should be addressed to Charles W. Solbrig; charles.solbrig@inl.gov

Received 28 March 2014; Accepted 23 July 2014; Published 17 September 2014

Academic Editor: Alexander B. Shick

The Zero Power Physics Reactor (ZPPR) operated from April 18, 1969, until 1990. ZPPR operated at low power for testing nuclear reactor designs. This paper examines the temperature of Pu content ZPPR fuel while it is in storage. Heat is generated in the fuel due to Pu and Am decay and is a concern for possible cladding damage. Damage to the cladding could lead to fuel hydriding and oxidizing. A series of computer simulations were made to determine the range of temperatures potentially occuring in the ZPPR fuel. The maximum calculated fuel temperature is 292°C (558°F). Conservative assumptions in the model intentionally overestimate temperatures. The stored fuel temperatures are dependent on the distribution of fuel in the surrounding storage compartments, the heat generation rate of the fuel, and the orientation of fuel. Direct fuel temperatures could not be measured but storage bin doors, storage sleeve doors, and storage canister temperatures were measured. Comparison of these three temperatures to the calculations indicates that the temperatures calculated with conservative assumptions are, as expected, higher than the actual temperatures. The maximum calculated fuel temperature with the most conservative assumptions is significantly below the fuel failure criterion of 600°C (1,112°F).

1. Introduction

ZPPR (Zero Power Physics Reactor) was the largest of the split-table fast reactor critical facilities. ZPPR was operated as a criticality facility from April 18, 1969, until being decommissioned in 1990. It was used to obtain a large amount of very detailed data on a variety of full-sized reactor configurations including large, commercial-sized fast reactors with powers of up to 1200 MW (electric). The purpose was to construct assemblies that closely resembled various fast reactor designs and then use the experimental results to validate and refine the data and methods used to design large fast reactors. There were 21 major assemblies, most of which had several major variants (e.g., beginning of cycle, middle of cycle, end of cycle, various control rod positions, etc.). The experiment campaigns included several large plutonium reactors, engineering mockups for both major design concepts for the clinch river breeder reactor designs, larger fast reactor designs as part of the JUPITER collaboration with Japan, the SP-100 space reactor, and assemblies supporting the integral fast reactor design [1].

The ZPPR critical assembly is put together from rectangular building blocks of fuel, coolant, and structural materials inserted into drawers. Figure 1 shows a picture of the ZPPR with a technician inserting material into the drawers in the left half of the reactor. The two halves of the reactor are identical. The reactor is in two sections which are closed up to bring the reactor to criticality for measurement of the neutron flux. There is a very large inventory of critical facility materials that can be assembled in various combinations to construct any reactor within just a few weeks. Because ZPPR was operated at very low power, the materials did not become very radioactive, and they were used over and over again. This feature, combined with the short time required to assemble a core, meant that nuclear reactors could be built and tested in ZPPR for about 0.1% of the capital cost of construction the whole power plant. The fuel was manufactured in 1967 and has been in storage since the reactor was decommissioned. So although the reactor has been decommissioned, the fuel must still be stored and maintained. Heat is generated in the fuel due to Pu and Am decay. The maximum temperature of these fuel elements caused by this heat generation as well as the

Figure 1: Experimenter loading fuel in the ZPPR.

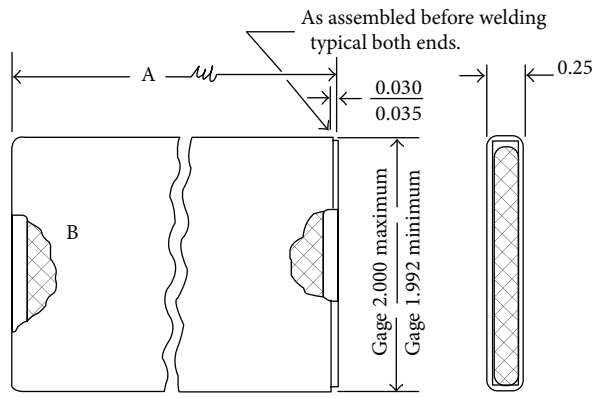

Figure 2: Schematic diagram of the ZPPR fuel elements.

Figure 3: Open clamshell with some fuel elements.

possible damage this temperature could cause to the cladding is the subject of this paper. Any damage to the cladding would be expected to lead to the fuel hydriding and oxidizing over the long period of storage as was observed in the damage to the ZPPR uranium fuel resulting in the fuel becoming unusable and a large potential source of contamination [2]. The objective of this paper is to analytically estimate the maximum temperature of the ZPPR stored fuel and to verify the results with sufficient certainty with the few temperature measurements that it is possible to make so that a conclusion can be drawn about whether cladding damage due to the thermal storage conditions has or has not occurred without physically examining the fuel.

The fuel, shown schematically in Figure 2, consists of metallic fuel bars (shown in cross hatching), 1.93 inches wide and 0.2025 inches thick encased in 15 mil thick 304L stainless steel cladding. The overall length of the fuel element, shown in the diagram as A, can be any whole number of inches from 1 to 9. The fuel length is 0.2 inches less than the length of the cladding.

The fuel elements are stored in aluminum clamshells as shown in Figure 3. The clamshell bottom has posts which cause the fuel plates to stand upright and keep the plates from touching one another. The clamshell top is shown in the background. The gasket fits in a groove for sealing when the clamshell is closed up.

When loaded in one direction, a clamshell can hold up to 12 eight-inch-long fuel plates, and in the other way it can hold up to 16 six-inch-long fuel plates. The posts in the clamshells used to store plates are set up to contain sufficient spacing for 1/4-inch plates. The plates shown in Figure 3 are 1/8-inch plates which are stored as two plates touching each other. The high Pu 240 plates used for bounding calculations in this paper are Pu-U-Mo plates which are 1/4 inches thick. The plates do not fit tightly and lean against the tapered pins so do not make good thermal contact with the clamshell.

Clamshells are stored in 4 inch-high by 8 inch-wide steel sleeves embedded in concrete as illustrated in Figure 4. Some of the clamshells, A, have rubber pads to prevent fuel damage from handling but they act as an insulator causing the fuel temperature to be higher. The fuel, B, is 2 inches high and the inside height of the clamshell is 2.25 inches.

A picture of the storage bins is shown in Figure 5. The bins are large rectangular concrete blocks, 27 inches deep, 32 inches wide, and 76 inches tall. Each bin contains twelve 8× 4-inch rectangular steel tubes, 0.188 inches thick, which run all the way through the structure. The 12-tube configuration is six vertical by two horizontal. Each tube can contain two ZPPR fuel storage containers (clamshells) sitting back-to-back with no separation.

Each storage sleeve (cavity) is closed by small individual steel doors on each end. Large steel security doors on each end provide a single closure that covers all the individual openings at once (see Figure 5). The doors are approximately 26 inches wide, 70 inches tall, 3 inches deep, and constructed of 3/16-inch sheet steel. The doors have piano hinges that are welded to the door and steel structure embedded in the bins.

The bin is all concrete. Figure 5 shows a long (72 inch) steel security bin door attached to the steel frame which is fastened to the concrete bin front. The door prevents opening of the 12 storage sleeves when it is closed and locked. Both ends of the bin have a security door which encases a 3-inch deep air space when closed. Figure 5 also shows that there are many storage bins lined up next to each other.

The combination of the 27-inch deep and 72-inch high concrete bins covered by security doors abutted to security bins on each side makes for highly insulated fuel elements and potentially high temperature fuel elements heated by the decay heat from the plutonium in the fuel.

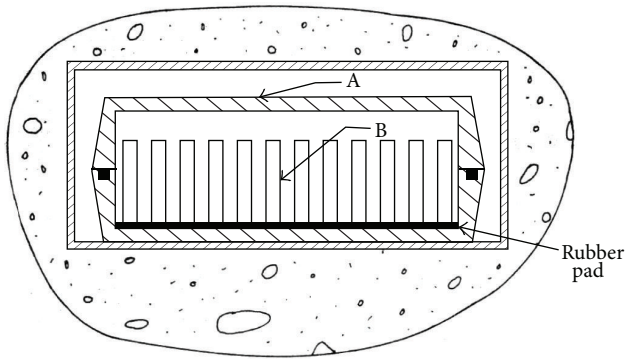

Figure 4: Clamshell with 12 eight-inch fuel elements perpendicular to front of storage bin.

Figure 5: Concrete storage bins with three-inch deep security doors.

Dimensions of a clamshell are shown in Figure 6. The criticality limit that controls the number of fuel elements allowed in a clamshell is 2,700 gm of the Pu-239 and Pu-241 in a clamshell [3]. The weight of Pu-239/241 in the fuel elements is 27.44 gm/inch. This corresponds to 98.40 inches of fuel and is large enough that the clamshell can be fully loaded with either twelve 8-inch fuel elements or sixteen 6-inch fuel elements (96 inches of fuel) which is the maximum fuel elements that can fit in the clamshell.

2. Background Information for Input Model

The base heat transfer model considers a single clamshell inserted in a closed fuel storage cavity with the cavity and bin doors closed. In order to make the calculation tractable, the heat transfer region analyzed is segregated from the rest of the storage bins by considering that adiabatic planes exist at the back of the clamshell (i.e., half way through the storage bin) and in the concrete 4 inches above, below, and from the sides of the cavity steel liner. This is a good assumption in those bins where all the fuel and the clamshell loadings are identical in each cavity. Since a majority of the clamshells do not contain heat generating elements, for example, the uranium fuel (which generates minimal heat) and nonfuel metal elements, the temperatures calculated will be necessarily higher than actual experience. That is, these nonheat or lower heat generating elements will act as heat sinks to the high Pu heat generating elements. As long as the fuel temperatures calculated with this model are acceptable, it is not necessary to go to a more detailed heat transfer model based on actual fuel distributions. The effect of these heat sinks was estimated in two computer runs. This effect is estimated simply by assuming the adjacent cavities have no heat generating clamshells.

Reasonable results were achieved when all the major heat transfer paths were finally represented. Leaving out any major heat transfer path resulted in bin and cavity doors and clamshell temperatures which are much higher than expected. Such unreasonably high temperatures imply that the fuel element temperatures would also be unreasonably high. So the current model is the simplest model which yields close to what the authors consider realistic temperatures, although they are still high. The comparison of calculated and measured bin door, cavity door and clamshell temperatures have shown that the fuel temperatures calculated with this model are conservatively high.

The largest heat generation rates occur in the high concentration of Pu fuel elements designated as PUMH (plutonium, uranium, molybdenum) in Klann, 2001. The maximum heat generated is in clamshells which are full of this PUMH fuel. In order to be full, all the fuel elements in the clamshell must contain either sixteen 6-inch-long elements (placed parallel to the bin door) or twelve 8-inch-long elements (placed perpendicular to the bin door). Both configurations yield the same total fuel length ($16 \times 6 = 96$, $12 \times 8 = 96$).

There are four types of fuel elements that can fill a clamshell. The highest heat generation rate is in the PUMH fuel which has a heat generation rate of 2.13 W/kg for a total heat load in a full clamshell of 23.1 W. The remaining three types have heat generation rates of about 0.98 W/kg and a total heat generation of about 10.5 W for a full clamshell. The expected temperatures for both the PUMH fuel and the lower heat generating fuel are estimated in this paper. It would take an extremely long time for a clamshell full of fuel elements placed in a cavity to heat up the concrete of the storage bins to come to equilibrium. On the order of weeks, since the fuel has been sitting in the bins for a much longer time than that, steady-state equilibrium temperatures are expected and are of most interest.

The fuel compositions are based on the 2001 report [4] and are the estimated compositions a bit before January 1, 1977. If all of the Pu-241 (half-life 14.4 years) had decayed to Am-241, the heat generation rate for the PUMH fuel would be 36.8 W instead of 23.1 W. A case with 35 W was run to scope the temperatures for a clamshell full of this 6-inch-long fuel. The heat generation rate in 2012 was estimated to be slightly less than 34 W (OriginZPPR-Max-DecayHeat.xlsx). Since the above compositions correspond to a lower heat generation rate than that which exists today, the base case heat generation rate actually corresponds to a partially full clamshell. The case with a heat generation rate of 35 W is also included in the analysis so that comparisons may be made between clamshells with different power levels. The January 1, 1977,

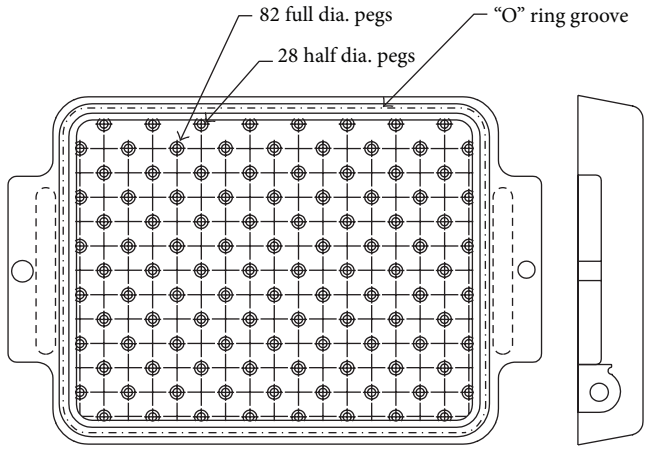

Figure 6: Planar view of lower section of empty clamshell.

concentrations are used for determining that the amount of fuel does not exceed the criticality limits. This is safe since the effective neutron multiplication factor of Am-241 is less than that of Pu-241.

3. Temperature Results of Fuel in Various Storage Conditions

The base model analyses a storage bin full of clamshells which are all the same and completely full of 6-inch fuel elements (of the composition identified in Klann et al. [4] Table 65 as PUMH [Pu, U, Mo] fuel). This symmetry allows a single storage cavity to be analyzed. That is, the single cavity can be analyzed as if it is insulated from the others. This will produce higher temperatures than the case where adjacent storage cavities may include few or no heat generating fuel elements. There is apparently no specified order in the storage of the fuel so that a random placement of clamshells in the storage cavities must be taken into account. Therefore, the maximum potential temperature must be analyzed, which is done with this selection.

Clamshells will only fit lengthwise into the storage sleeve. The end closest to the bin door is termed the front end and the other the back end. The analysis assumes a clamshell loaded with 6-inch fuel elements placed parallel to the bin front and with the back end of the clamshell insulated. The back end insulation occurs because of symmetry; that is, the storage cavities contain two clamshells back to back loaded with the same loading pattern and amount of fuel. This symmetry requires that the highest temperature is the last fuel element in the clamshell. As an approximation, the back of the last fuel element is considered insulated no matter how many fuel elements are in the clamshell. This approximation is tested in parametric studies.

The heat transfer is represented in two dimensions, one vertical, the other along the horizontal depth of the cavity. The heat transfer out the vertical sides of the storage cavities is estimated by increasing the thermal conductivity of the steel sleeve and the concrete. Although this distorts transient calculations a bit, steady-state temperatures are only dependent on the thermal conductivities and not the densities or specific heats. Also, the identical storage cavities above and below indicate there would be adiabatic surfaces above and below each cavity, which are estimated to be midway between the clamshell cavities. The vertical distance between the storage cavities is 8 inches. The adiabatic top boundary is estimated to be 4 inches above the top of the cavity, and the adiabatic bottom boundary is estimated to be 4 inches below the bottom of the cavity. With all the other surfaces insulated, the bin door boundary is the only one through which the heat generated by the fuel is transferred to the storage room. This boundary is the outside of the bin storage door. The properties of the material used are listed below. The January 1, 1977, fuel composition was approximately 34.9% Pu and 65.1% U with a small amount of Am and Mo. The Pu and U percentages are used to estimate the properties of the fuel. The decay of Pu-241 to Am-241 is not taken into account in the material thermal properties.

The heat transfer through the cavity door and bin facial concrete contains many difficult paths to analyze. The bin door covers a two horizontal by six vertical matrix of cavity doors and encloses a 3-inch deep air space between bin concrete face and inside bin door. This air space is not air tight so some air can come in the bottom of the space and flow out the top due to buoyancy. It is at a lower temperature at the bottom and heats up as it rises. This effect is not explicitly considered but is small in comparison to the uncertainty of estimating the Nusselt number between the storage sleeve doors and bin door. The bin door frame is attached to the concrete bin face in a nonsymmetric manner and is only approximately represented. This geometry introduces the most uncertainty of all the other factors in the fuel temperature estimation. Elements of the geometry are introduced in the model in ways meant to overestimate the fuel temperature. The discussion of uncertainties in this representation and the comparison of measured temperature uncertainties are included in latter sections.

The thermal properties used in the analysis are included in Table 1. Material properties were obtained from the

Table 1: Thermophysical properties used in analyses.

Material number	Specific heat J/kg °C	Thermal conductivity W/m °K	Density gm/cc	Material
1	910	237	2.7	Aluminum
2	1008	0.02	0.001	Air Nu = 1
3	123.49	20.25476	19.3443	0.349 Pu, 0.651 U fuel
4	460	43 ∗ 1.66	7.85	$K_{\text{lower steel}}$
5	890	1.1 ∗ 3.0	2.1	$K_{\text{lower concrete}}$
6	1008	0.02 ∗ 11.8	0.001	Air Nu = 11.8
7	460	43 ∗ 2.33	7.85	$K_{\text{upper steel}}$
8	880	1.1 ∗ 3.66	2.1	$K_{\text{upper concrete}}$
9	1008	0.02 ∗ 4	0.001	Air Nu = 4
	130	6.74	19.8	Pu
	120	27.5	19.1	U

Table 2: Fuel properties used in the analysis for PUMH fuel.

	gms	W/kg	W	Element Wt	Wt fraction	Fuel dimensions		
Pu238	0.2676	567	0.151729			Plate Thk =	0.2025	in
Pu239	209.1584	1.93	0.403676			Height =	1.93	in
Pu240	80.4538	7.1	0.571222			Length =	7.802	in
Pu241	10.3554	3.39	0.035105			Vol. of plate	3.049217	in^3
Pu242	4.3821	0.12	0.000526	304.6173	0.337627	Vol. of plate	49.96771	cm^3
Am241	6.6815	114	0.761691	6.6815	0.007406	Mass	902.2299	gm
U235	1.1998	0.0142	$1.7E-05$			Area	97.14729	cm^2
U238	567.174	0.0001	$5.67E-05$	568.3738	0.629966	Clad thick	0.015	in
Mo	22.5573	Tot. Watts =	1.924022	22.5573	0.025002	Weld thick	0.02	in
Total Wt (gm)	902.2299	Tot. W/kg =	2.132519	Pu239/241	Pu/(Pu + U)	Weld area	0.0853	in^2
Dens. gm/cc	18.05626	W for 12	23.08827	219.5138	0.348935			

Weight data from Table 65 for 8-inch-long NUMH fuel, of Klann (2001) [4].

internet. No specific reference is included because that would imply that the values are universally agreed upon but, in fact, they vary from one reference to another (in the range of 20%). There is also uncertainty as to what specific material was used in construction. For example, the concrete conductivity, k, used here (1.1 W/m °K) is for dense concrete. The k of dense concrete is listed as between 1.0 and 1.8 W/m °K in http://www.engineeringtoolbox.com/thermal-conductivity-d_429.html. The bin concrete includes 3.8% boron frit. Since the conductivity of this concrete is a significant factor in determining the clamshell and fuel temperature, it may be judicious to determine this property more accurately.

Note that the thermal conductivity of air for $m = 6$ and 9 in Table 1 has been increased by the Nusselt number to represent increased heat transfer in the air spaces due to natural circulation. The thermal conductivity of the steel sleeve, the doors, and the concrete has been increased by factors in $m = 4, 5, 7$, and 8 to simulate the third dimension heat transfer. Note that the conductivities of these materials in Table 1 are presented in the form of a multiplier times the actual material conductivity to account for natural circulation or 3D heat transfer.

Detailed composition and heat generation rates for each isotope in the PUMH fuel are included in Table 2. (Note that the weld area in this table is not the total weld area of the fuel element but the weld area associated with the pressure that would apply a force in the axial direction.)

The properties of the 8-inch-long fuel plates (PUMH) above were used in the following analysis but modified for the shorter 6-inch plates. The extensive properties are proportional to length; the intensive are the same as the 8-inch fuel.

The input material description for the 6-inch plates is included in Figure 7. The numbers along the top and left side are indices for the regions and surfaces in the model. The numbers in the region correspond to the materials defined in Table 1. Only the geometry from the outer door to the back of the first 7 fuel elements is shown but 16 fuel elements are included in the model. The remaining geometry not shown is modeled the same as the geometry of the seven shown in Figure 7. Note that thermal radiation is included between all parallel surfaces which are separated by an air space.

The input from outside the bin door to the sleeve door in Figure 7 is based upon the geometry described in the introduction, especially in Figures 4, 5, and 6. Since the fuel elements are metallic with high conductivity, the fuel element composition is approximated as containing only Pu and U

	1	2	3	4	5	6	7	8	9	10	11	12	13	14	15	16	17	18	19	20
1	4	4	8	8	8	8	8	8	8	8	8	8	8	8	8	8	8	8	8	8
2	4	6	8	8	8	8	8	8	8	8	8	8	8	8	8	8	8	8	8	8
3	4	6	4	7	7	7	7	7	7	7	7	7	7	7	7	7	7	7	7	7
4	4	6	4	2	9	9	9	9	9	9	9	9	9	9	9	9	9	9	9	9
5	4	6	4	2	2	1	1	1	1	1	1	1	1	1	1	1	1	1	1	1
6	4	6	4	2	2	1	2	2	2	2	2	2	2	2	2	2	2	2	2	2
7	4	6	4	2	2	1	2	3	2	3	2	3	2	3	2	3	2	3	2	3
8	4	6	4	2	2	1	2	2	2	2	2	2	2	2	2	2	2	2	2	2
9	4	6	4	2	2	1	1	1	1	1	1	1	1	1	1	1	1	1	1	1
10	4	6	4	2	2	2	2	2	2	2	2	2	2	2	2	2	2	2	2	2
11	4	6	4	4	4	4	4	4	4	4	4	4	4	4	4	4	4	4	4	4
12	4	6	2	2	2	2	2	2	2	2	2	2	2	2	2	2	2	2	2	2
13	4	6	5	5	5	5	5	5	5	5	5	5	5	5	5	5	5	5	5	5
14	4	4	5	5	5	5	5	5	5	5	5	5	5	5	5	5	5	5	5	5

Fuel
Aluminum
Air
Steel
Concrete

(1) Aluminum
(2) Air Nu = 1
(3) Pu U Mo
(4) $K_{\text{lower steel}}$
(5) $K_{\text{lower concrete}}$
(6) Air Nu = 11.8
(7) $K_{\text{upper steel}}$
(8) $K_{\text{upper concrete}}$
(9) Air Nu = 4

Figure 7: Material input.

Figure 8: Heat flow path from storage sleeve through concrete to the bin door.

metals and the details of the stainless steel cladding are not modeled. The bin door geometry causes the modeling of the heat transfer out of the front of the bin to be complicated. The storage sleeve and its metal door conduct heat directly to the concrete. The heat is conducted through the concrete to the bin door frame and then to the metal bin doors. The storage sleeve door and the face of the concrete convert and radiate heat to the bin door which is normally closed.

This concrete contacts the steel frame of the bin door. Figure 8 gives a better view of how the metal bin door frame interacts with the concrete and embedded storage sleeve and its door.

The metal frame which supports the bin doors contacts the concrete over a 1-inch width. Even though the conduction path is less than 1-inch-thick steel, the conductivity of steel is so high that this conduction path will conduct all the heat from the wider contact area, so it is more important to represent the contact area between the metal and concrete than the heat transfer thickness. The contact area in the model is located 3 inches from the storage sleeve on both the upper and lower ends of the model, but the actual geometry is much more complicated.

Each of the subregions shown in Figure 7 is subdivided as well. The increments used in each subregion of Figure 7 are shown in the second row and in the first column in Figure 9. The width and thickness of each region are shown as well.

The coefficient representing heat transfer from the storage bin surface to the storage room is taken as 100 W/m^2 °K The storage room temperature is usually kept at 35°C (95°F) by a thermostat controlled cooling system.

As mentioned previously, each storage cavity is insulated from the others except for problems in which the neighboring empty cavities are included in the analysis. Also, the back of the last fuel element in this model is specified as insulated. It is more accurate to represent the additional air space behind this fuel element and the end of the clamshell and then insulate the back of the clamshell. The former geometry has been used in most of the analyses. A case with the more accurate geometry has been run and shows that slightly higher temperatures (5°C [9°F] max) are obtained without the more accurate geometry so use of the simpler geometry predicts a slightly higher temperature.

3.1. Best Model (Conservative and Best Estimate) Steady-State Temperatures—High Heat Generation Fuel. This section presents results obtained with the best estimate input model

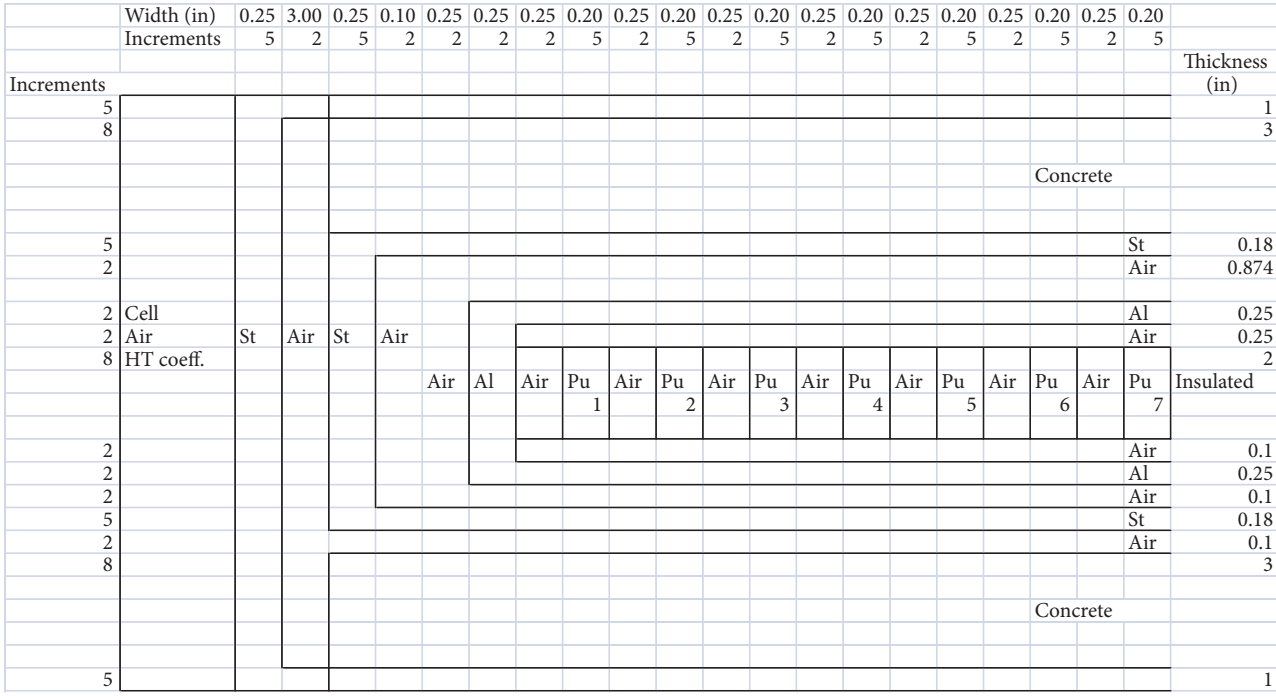

Figure 9: Increments used in each region and dimensions.

(as judged by the authors). The largest conservative factor in this model is the surface contact resistances. Conservative and best estimate values of the resistances are presented in this section. One nonconservative value for the decay heat is used here. This nonconservatism is investigated in the parametric study in Section 3.2.

There is a desire to produce conservatively high temperatures in these studies. If the results show that the fuel is not damaged with the conservative results, then it can be concluded that no damage to the fuel will occur at the lower storage temperature. This objective is met by assuming high heat transfer resistances for surfaces in contact with each other. There is also a desire to produce close to realistic results. This objective can be approached with more realistic assumptions for these resistances. Three cases are investigated in this section. The first case (base Case A) uses high heat transfer resistances. Case B uses intermediate resistances and Case C uses low resistances.

3.1.1. High Heat Transfer Resistances. The steady-state center line fuel best estimates temperatures for a clamshell full of 6-inch high heat generation PUMH fuel for a total heat generation in the clamshell of 23 W and a specific heat generation rate of 2.13 W/kg is shown in Figures 10 and 7. Room temperature is 35°C (95°F). The bin door temperature is 38.7°C (101.7°F). The inner door is at 74.8°C (166.6°F), and the clamshell is at 106.6°C (223.9°F). The latter two temperatures would be high enough to require protective gloves but the maximum temperature is not high enough to damage fuel.

The temperature distribution on a horizontal plane through the center of the fuel is shown in Figure 11. The maximum fuel temperature is 185.8°C (366.5°F). There is a significant increase in the fuel element temperature for the first three elements over the temperature of the clamshell but the fourth and the following all are near the maximum temperature (last). All the fuel elements from four to sixteen are above 174.6°C (346.3°F).

The vertical and horizontal temperature fields are shown in Figure 12. It is interesting to note that the clamshell temperature, shown as being 106.6°C (223.9°F) in Figure 11, is almost constant spatially. This is because the thermal conductivity of the aluminum clamshell is so high compared to the other conductivities. In fact, increasing its thermal conductivity would not change the solution much at all.

Figure 13 shows the uniformity of the clamshell top and bottom of the clamshell in spite of the fact that the fuel temperature rises so drastically. This implies that the average temperature of the clamshell is only dependent on the total heat generated by the fuel and not on the distribution of the fuel temperature.

3.1.2. Lower Heat Transfer Resistances (Higher Conductances), More Realistic Model

Case A. One of the most conservative factors introduced into the model is the interface heat transfer resistance. The resistance between two surfaces used in the above base model results from an assumed air space of $\Delta = 0.1$ inches between the surfaces. The air space is equivalent to an interface

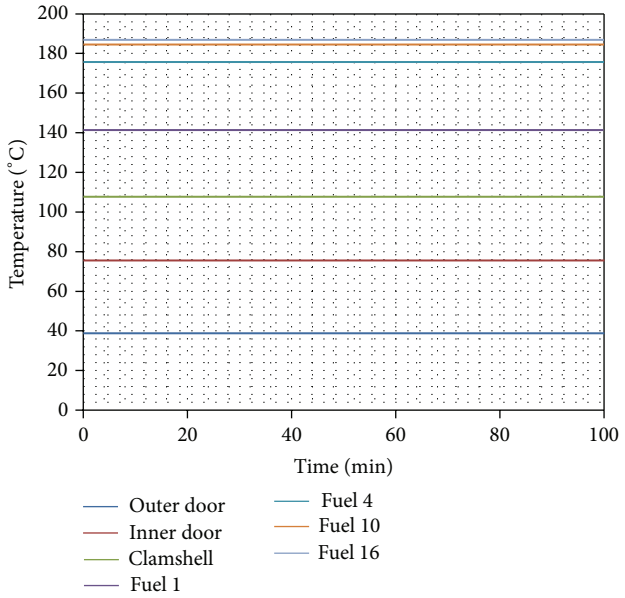

FIGURE 10: Temperatures at specific locations of high heat generation PUMH fuel.

FIGURE 11: Temperature on plane through center of fuel high heat generation PUMH fuel.

heat transfer coefficient of 7.9 W/m^2 °K as calculated by the equation:

$$h = \frac{k_{\text{air}}}{\Delta} = \frac{0.02\ (\text{W/cm}^\circ\text{K})}{0.1 * 0.0254\,\text{m}} = 7.9 \frac{\text{W}}{\text{m}^2\,^\circ\text{K}}. \quad (1)$$

This model has been used in three places: the placement of the clamshell on the inside of the sleeve and the placement of the fuel on the surface of the clamshell. In addition, the bottom portion of the sleeve has been assumed to be separated from the concrete and to have this 0.1-inch air space. More realistic values for each of these locations are considered in this section.

Case B. The clamshell is placed on the sleeve surface with no pressure except the weight of the fuel-filled clamshell which results in a no pressure interface heat transfer coefficient.

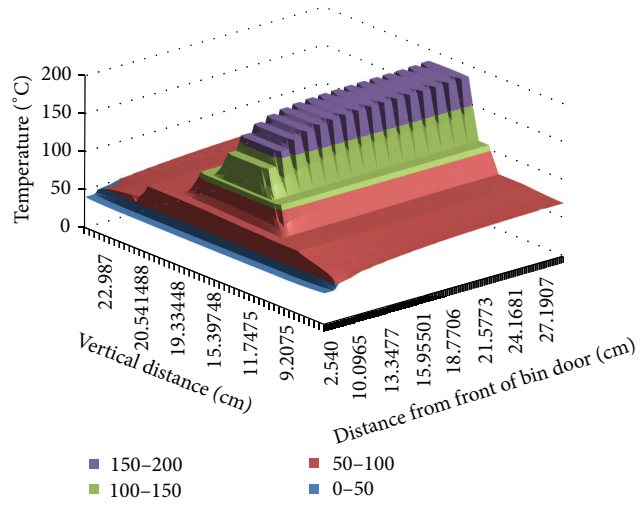

FIGURE 12: Entire temperature field high heat generation PUMH fuel.

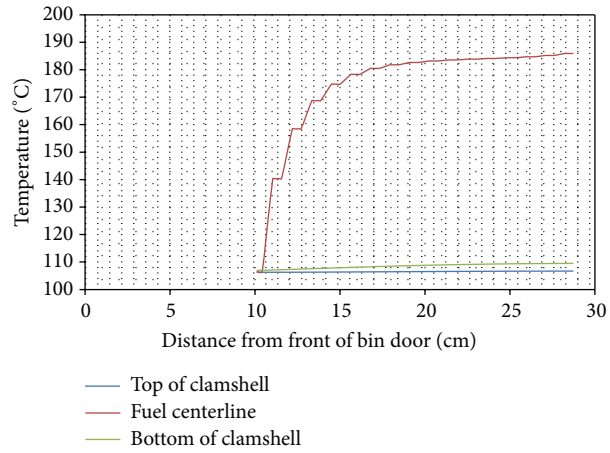

FIGURE 13: Uniformity of the temperature of the clamshell.

The value used between the clamshell and the sleeve is consistent with the zero pressure value presented in [5] which is 1,968 W/m^2 °K. The same value has been used in the space between the sleeve and the concrete. The original conservative value of 7.9 W/m^2 °K is used for the fuel contact with the clamshell.

The results for Case B are shown in Table 3 where it is compared to the base case. It is noted that the clamshell temperature decreases almost 30°C. The inner door temperature decreases 6°C. All fuel temperatures decrease about 23°C. The maximum fuel temperature is 163°C.

Case C. In this case, the heat transfer resistance of the contact between the fuel and the clamshell is reduced along with the reductions of Case B. There is a large uncertainty in the contact resistance between the fuel and clamshell. The fuel is placed in the clamshell with no downward pressure other than gravity. It can lean against the tapered support posts in the clamshell so that the bottom of the fuel may only contact

Table 3: Comparisons of results of the various heat transfer resistances (°C).

	Storage room	Outer door	Inner door	Clamshell	Fuel 1	Fuel 4	Fuel 10	Fuel 16
Distance from front of bin door (cm)	0	0.25	8.51	10.10	11.25	14.81	21.88	28.74
Conservatively h in three interfaces-base Case A	35.0	38.7	74.8	106.6	140.3	174.6	183.5	185.8
High h clamshell to sleeve and sleeve to concrete B	35.0	38.7	68.6	77.1	114.1	150.8	160.3	163.2
Same as above and Med h fuel to clamshell C	35.0	38.7	68.1	75.9	96.7	111.6	114.8	116.2

the clamshell along its edge. It may lean against one or more posts which can transfer some heat.

The following model is used to estimate the effective interface heat transfer coefficient between the fuel and clamshell. The two surfaces of the metals have a roughness so contact each other only on the crests of these bumps and only when the crests are in the same place. That is, many of the crests are unable to touch because one metal has a crest at the location that the other has a valley. The heat transfer through the metal areas that contact each other where F is the fuel, C is the clamshell, and T^* is the intermediate temperature where they contact is given by

$$Q_M = \frac{k_F}{\Delta/2} A_M \left(T_F - T^*\right) \qquad Q_M = \frac{k_C}{\Delta/2} A_M \left(T^* - T_C\right), \tag{2}$$

where Δ is the space between fuel and clamshell.

Eliminating the intermediate temperature T^* yields the following:

$$Q_M = \frac{2}{1/k_F + 1/k_C} \frac{A_M}{\Delta} \left(T_F - T_C\right), \tag{3}$$

where A_M is the metal contact area.

The heat transfer through the air portion, A_A, is given by

$$Q_A = \frac{k_A}{\Delta} A_A \left(T_F - T_C\right). \tag{4}$$

Combining (3) and (4) together gives the total heat transfer across the surface and allows an effective interface heat transfer coefficient, h_{int}, to be defined below:

$$\begin{aligned} Q_{\text{Tot}} &= Q_M + Q_A \\ &= \left\{ \frac{2}{1/k_F + 1/k_C} \frac{P_M}{\Delta} + \frac{k_A P_A}{\Delta} \right\} A_{\text{Tot}} \left(T_F - T_C\right) \\ &\equiv h_{\text{int}} A_{\text{Tot}} \left(T_F - T_C\right), \end{aligned} \tag{5}$$

where P represents the area fractions of the metal and air. The percentage of metal is assumed to be very small and it is taken in this case to be 0.22% to yield an h_{int} of 40 W/m^2 °K.

Case C results in Table 3 indicate a decrease in the maximum fuel temperature of 47°C over that of Case B. This is a significant drop in the temperature from a small contact area. The model assumes that in this small contact area there is no heat transfer resistance between the touching metals. In order to estimate a temperature above the actual temperature, it is safer to assume that the fuel clamshell interface has the large resistance assumed in base Cases A and B.

An important item to notice from comparing the base Cases A and B is that temperature measurements of the outer bin door, the inner sleeve door, and the clamshell would show a measurable difference between the high and low heat transfer resistance for the clamshell to sleeve and sleeve to concrete cases interfaces.

It was hoped that these measurements could be used to infer the conservatism in the fuel temperature measurement; however, this is not the case but it can possibly bracket the fuel temperature. It is observed that, in Table 3, the temperatures of the outer door, inner door, and clamshell are the same for Cases B and C despite the fact that there is a large difference in the fuel temperatures. As will be shown in the data comparison section, the three measured temperatures agree with Cases B and C. Although the fuel interior temperature cannot be determined from this measurement, it can be bracketed since it is unlikely that the fuel temperature would be higher than that shown in Case B since the assumed interface heat transfer is so low in that case. It would not be as high as Case A because the measured temperatures are lower than Case A.

3.1.3. Effect of Modifying the Thermal Conductivity of Steel and Concrete. Another important assumption introduced into the model is the amplification of the conductivity in the concrete and steel to take into account the third dimension of heat transfer. The conductivity factor has been reduced to 1 for the concrete and steel (materials 4, 5, 7, and 8) to determine its effect for Case A and Case C. The comparisons are shown in Table 4. For the high resistance case the fuel increases 16°C (compare A to A1) but the increase is more pronounced in 27°C in the low resistance case (compare C to C1).

3.2. Parametric Studies. Parametric studies were conducted using a preliminary model for the base case. The preliminary base case yields slightly higher temperatures than the best model but the effect of the parameter changes should be similar. The first eleven cases analyzed six-inch fuel elements parallel to the storage sleeve door. The high heat transfer resistances of the first best estimate case have been used in these studies. The cases analyzed are

(1) high heat generation fuel, PUMH (base case),

(2) higher fuel emissivity,

(3) lower heat generation fuel,

(4) high power, no heat generation in neighboring cavities, and PUMH fuel,

(5) low power, no heat generation in neighboring storage cavities,

Table 4: Effect of setting thermal conductivity amplification factors to one (°C).

	Storage room	Outer door	Inner door	Clamshell	Fuel 1	Fuel 4	Fuel 10	Fuel 16
Distance from front (cm)	0	0.25	8.51	10.10	11.25	14.81	21.88	28.74
Case A	35	39	75	107	140	175	183	186
Case A1	35	40	94	127	158	191	200	202
Case C	35	39	68	76	97	112	115	116
Case C1	35	40	90	103	123	138	142	143

(6) no thermal radiation,

(7) rubber pad inserted on bottom of clamshell,

(8) only six fuel elements,

(9) cell cooling being turned off,

(10) higher power due to decay of Pu-241 to Am-241,

(11) higher power plus cell cooling being turned off,

(12) 8-inch fuel elements perpendicular to cavity door.

A summary of the parametric study is presented in Table 5. Eleven of the cases investigated were for clamshells with 6-inch fuel elements placed parallel to the bin door. The last was for elements perpendicular to the bin door. In most cases, only steady state results were obtained. In two cases, transient as well as steady state results were obtained.

The maximum fuel temperature for the high power preliminary base case (Case 1) with the PUMH fuel and fuel emissivity of 0.3 is 220°C (428°F). The cavity door temperature is 87°C (189°F), and the clamshell temperature is 147°C. Case 1 also shows that clamshell temperature is almost uniform which allows the problem to be split into two: the determination of the clamshell temperature based upon the total heat generation and the determination of the fuel temperature knowing the clamshell temperature. This is discussed more later in this section.

Using a higher fuel emissivity of 0.8 (Case 2) yields a lower temperature of 192°C (378°F), but the lower emissivity of 0.3 for the shiny cladding is considered to be more realistic.

The temperatures are much lower for the lower power clamshells with Pu containing fuel with a power density of 0.99 W/kg as shown in Case 3. These results may be more representative of most of the fuel than the high power in Case 1. The fuel temperatures are less than 140°C (284°F).

The temperatures would be lower if the neighboring cavities had lower power generation. This is checked out in Case 4 where Case 1 was rerun with zero power in the adjacent cavities.

The low power case, Case 3, was rerun with no heat generation in neighboring cavities as Case 5.

Some clamshells contain a 1/16-inch rubber pad to prevent damage to the fuel. The insulating effect of this pad is estimated in Case 6. The properties used were for Rubber Silicone with C_p = 2010 J/kg°C, k = 0.13 W/m°K, and rho = 1.25 gm/cc. These are representative values and not particular to the actual pads. The pad raises the maximum fuel temperature by only 4°C (7.2°F) over Case 1. As expected, the inner door and clamshell temperatures remain the same because the heat generation rate is the same. The reason that there is no much effect is that the base case uses a large heat transfer resistance between the fuel and the clamshell.

Case 7 shows that including thermal radiation in the model is very important. The fuel temperature is much higher at 530°C (986°F) when thermal radiation is neglected. Thus, thermal radiation is extremely important in estimating these temperatures. It carries much more heat across the air spaces than the conduction and convection of air.

Case 8 shows that reducing the number of elements to six decreases the temperature of all the six fuel elements. The reason for this is that these fuel elements are no longer receiving heat from the elements seven to sixteen.

Case 9 considers the case where the storage room cooling is off. Experience has shown that the room temperature increases to a maximum of 150°F (65.5°C). Because thermal radiation is not linear, the maximum fuel temperature increases by only 15°C (27°F) even though the ambient temperature increases by 30.5°C (55°F). The transient behavior of this case is discussed later on.

Case 10 analyzes a clamshell where a significant amount of Pu-241 has decayed to Am-241. Calculations indicate that enough Pu-241 has decayed to Am-241; that is, the decay heat for a full clamshell in 2012 is almost 34 W. So a clamshell with 35 W heat generation was analyzed for Case 10. The maximum fuel temperature has increased to 280°C (536°F), an increase of 60°C (108°F) over the base of 220°C (428°F). This is still much lower than the 600°C (1,112°F) failure limit of the fuel. Both the cavity door and the clamshell temperatures have increased considerably.

Case 11 is Case 10 redone assuming the loss of cell cooling. The combination of the maximum heat generation and loss of cooling yields the maximum fuel temperature possible in storage. This temperature is 292°C (558°F). This is an increase of 12°C (22°F) over Case 10.

Case 12 estimates the temperature of the 8-inch fuel elements. Due to the high conductivity of the clamshell, the clamshell temperature only depends upon the total heat generated in the clamshell (as long as it is somewhat evenly distributed). This is verified by observing that the clamshell temperatures are the same for Cases 1, 2, and 6. They have the same heat generation, so the clamshell temperatures are the same even though the fuel temperatures are different. Since a clamshell fully loaded with twelve 8-inch fuel elements has the same total heat generation as the fully loaded clamshell with 6-inch fuel elements, the temperature of the 8-inch fuel elements was determined with a model that included only the clamshell and the fuel. The clamshell temperature was

Table 5: Summary of calculated fuel temperature results.

Case	Number of fuel plates	Problem description	Temperatures, ˚C Max fuel	Front clam	Cavity door	Bin door	Compare to	Max fuel Temp. diff. from base
Fuel placed parallel to front of storage bins—6-inch elements								
A	16	Base, eps = 0.3	186	107	75	39	Best Est.	Base case
1	16	Base, eps = 0.3	219.3	146.9	87	39.6	Base for	Parameter study
2	16	Increase eps = 0.8	191.6	147.7	87.4	39.6	Case 1	Minus 29
3	16	Low power	137.4	96.2	61.6	37.2	Case 1	Minus 83
4	16	No heat next cavity, high power	200.2	123.4	67	37.6	Case 1	Minus 20
5	16	No heat next cavity, low power	124.3	81.7	50.7	36.2	Case 3	Minus 13
6	16	Rub mat and Al plate	224.1	147.2	87.5	39.7	Case 1	Plus 4
7	16	No thermal radiation	530	392	185.8	39.5	Case 1	Plus 310
8	6	Only 6 fuel elements	182.8	110.1	58.4	36.8	Case 1	
9	16	Cell cooling off	235.3	166.3	111.6	70.2	Case 1	Plus 15
10	16	Hi power 35 W	280.4	186.8	109.2	42.1	Case 1	Plus 60
11	16	Hi power 35 W and cell cooling off	292	202	130.5	72.6	Case 1	Plus 72
Fuel placed perpendicular to front of storage bins—8-inch elements								
12	12	8-inch fuel	210	146.9	87	39.6	Case 1	Minus 10

specified to be the same as in Case 1. Case 12 shows that fuel elements placed perpendicular to the bin door produce maximum fuel temperature of 210˚C (410˚F) which is 10˚C (18˚F) lower than that in the base case (Case 1).

More detail is presented in the following for Case 1, Case 8, and Case 9.

3.2.1. Case 1: Effect of Adding the End of the Clamshell into the Model. As mentioned previously, the high thermal conductivity of the aluminum clamshell causes the clamshell to be at a near uniform temperature and indicates the possibility that adding additional convection and radiation heat paths between the last fuel plate and the end of the clamshell would reduce the fuel temperature. The more accurate detail was added to the model, and the modified results are shown in Figure 14. The temperature distribution is seen to be almost symmetrical, but the maximum temperature has only been reduced a small amount by the addition of this heat transfer path (219 [426] to 215˚C [419˚F]). Thus, it is concluded that it is not necessary to include this detail in the model.

There is still somewhat of an asymmetry because the clamshell temperature does increase 4˚C across the clamshell in the horizontal direction. To check on what the temperature would be if it were symmetric, a subset of this problem modeling just the clamshell assuming it was at a uniform temperature of 147 (297˚F). The results are shown in Figure 15. The result is symmetric, but the maximum temperature is still the same (215˚C [419˚F]). This result shows that if the clamshell temperature is known, the maximum fuel temperature can be estimated by just representing the clamshell and contents.

This also means that the temperature of the clamshell depends upon the heat generation and not on the temperature distribution of the fuel in the clamshell. Thus, the heat transfer problems can be separated into two analyses. A heat transfer analysis outside the clamshell with a specified heat generation within the clamshell would determine the clamshell temperature. This temperature could then be used to determine the temperature distribution in the fuel inside the clamshell. This fact was needed to determine the temperature of the eight-inch fuel elements placed perpendicular to the door in Case 12. That is, since a two-dimensional code is being used, the fuel placed perpendicular to the bin door would require a three-dimensional analysis. Since the two problems can be separated, a two-dimensional analysis, one in the vertical direction and another parallel to the bin door, was sufficient to determine these fuel temperatures. If the problems could not be separated, then a three-dimensional analysis would be required to represent the nonheat generating space between the fuel elements.

3.2.2. Case 8: Fuel Temperatures with Only Six Fuel Elements. The temperatures with only six fuel elements in the front part of the clamshell are described in this section, and the results are presented in Figure 16 using the same physical constants as the base Case 1. The maximum fuel temperature is 183˚C (361˚F) versus 219 (426˚F) for Case 1. The temperature for fuel element 1 has decreased to 142˚C (288˚F) from 180˚C (356˚F). This emphasizes that the temperature of all the fuel elements rises when additional fuel elements are added to a clamshell because some of the heat from the end fuel elements must travel through the fuel elements in front of it to escape from the clamshell.

3.2.3. Cell Cooling Fails or Is Turned Off. The steady state obtained with the storage room cooling fails or is turned off as shown in Figure 17. Experience has shown that, during loss of storage room cooling, the storage room reaches a temperature

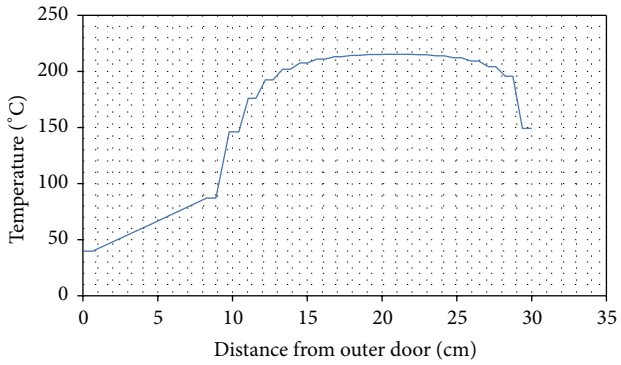

Figure 14: Temperature through center of fuel with end added to clamshell.

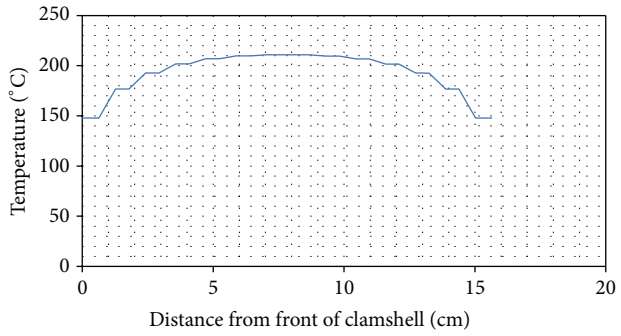

Figure 15: Temperature through center of fuel with a specified clamshell temperature.

of 150°F (65.5°C) and stays there due to heat loss through the walls. The transient behavior is calculated starting from the steady-state temperatures in the base case. The temperature behavior is shown for the first eight hours. The temperature rise rate is very slow. It is estimated that it would take at least 20 hours for this transient to reach steady state. The final steady-state temperatures assuming that the cooling is not restarted are also shown in this figure. If the cell cooling fails or is left off for about 20 hours, the fuel temperature will reach steady state.

4. Analytical Models Used in the Solution

The geometry that has been modeled is shown in Figures 7 and 9. Section 4.1 describes the modeling of each region by the conduction equation in two dimensions with heat generation in the fuel regions and with separate material properties specified for each region. The heat transfer between regions is represented by equating the heat fluxes at the interfaces and the addition of thermal radiation components at interfaces which include thermal radiation. Section 4.2 describes the modification of the thermal conductivity in the air regions which contain air instead of solid material to take into account natural circulation. Section 4.3 describes the method used to take thermal radiation into account across the air regions. Finally, the steel and concrete regions around the cavity provide extra capability to transfer heat away from

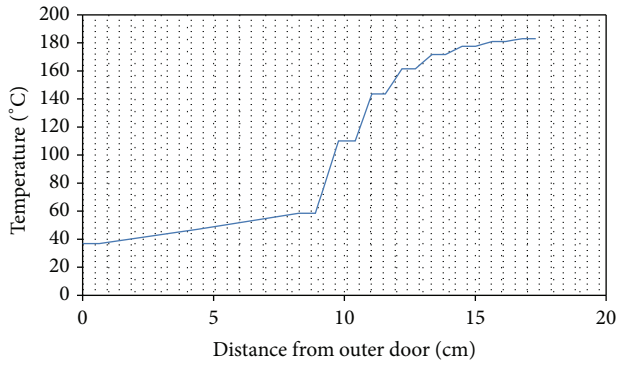

Figure 16: Centerline profile with only six fuel elements (ZPPR 2d 18 12 TRkRad1.xlsm).

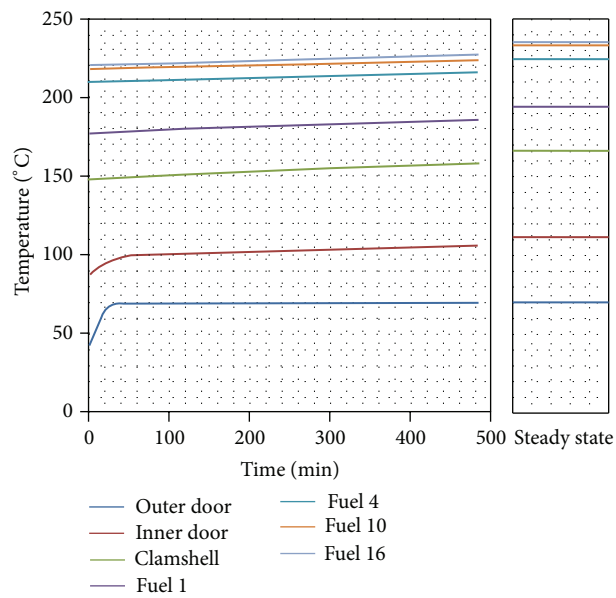

Figure 17: Storage room cooling fails off.

the clamshells, and modifications to the thermal conductivity have been made in these regions to simulate this additional heat transfer. These models are discussed in Section 4.4. The numerical effects of the conductivity amplification were presented in Section 3.1.3.

4.1. Conduction Model. The conduction equation for the temperature T in two dimensions in region "i" is given as

$$\rho_i C_{pi} \frac{\partial T_i}{\partial t} = k_i \frac{\partial^2 T_i}{\partial x^2} + k_i \frac{\partial^2 T_i}{\partial y^2} + q_i, \quad (6)$$

where ρ is the density, C_p is the specific heat, k is the thermal conductivity, q is the heat generation rate per unit volume, t is the time, x is the horizontal axis, y is the vertical axis, and i represents the region or material. The heat flux and temperatures at interfaces between solid bodies are equated. Modifications are made for at air spaces which radiate heat to other surfaces and these are described in Section 4.3.

The boundary condition on the outside bin door (specified to be the left boundary) is given as

$$k_s \frac{\partial T}{\partial x} = h_c \left(T - T_c\right), \tag{7}$$

where k_s is the thermal conductivity of the steel door, h_c is the heat transfer coefficient of the cell air, h_c is a function of the forced circulation of the cooling system, and T_c is the constant average temperature of the cell atmosphere kept at 35°C. The temperature derivative is evaluated on the right-hand side of the boundary. The air circulation system is assumed to provide adequate flow around the bins to yield a high heat transfer coefficient estimated at 100 W/m^2 °K. The upper and lower boundaries and the right hand boundary are insulated.

The solution method uses an explicit numerical transient solution for all interior nodes. The boundary nodes are solved for after the interior nodes and since the interior temperatures are known, the only unknowns in the boundary equations are the boundary temperatures which are solved for explicitly.

4.2. Natural Convection in the Air Spaces. The Nusselt number is to be used as a multiplier to indicate how much the effective conductivity of air is increased due to natural circulation. When Nu = 1, the heat transfer is just simple conduction of stationary air. The Nusselt number must be greater than or equal to one.

In this section, literature values for heat transfer in spaces similar to those encountered in the ZPPR storage were evaluated. This evaluation shows that the Nusselt number in the air space between the bin and cavity doors is large (Nu = 11.5) but small in the spaces around the fuel (Nu = 1) and Nu = 3 in the space above the clamshell.

Experiments and analysis are used to determine the enhancement of the heat transfer coefficient, h, by free convection over that of static air [6, 7]. If the effective thermal conductivity, k_e, across an air space is a_k times that of static air, k_a, then the Nusselt number will equal a_k. So by realizing that h across an air gap is the effective conductivity divided by the distance, d, across an air gap,

$$h = \frac{k_e}{d} = \frac{a_k * k_a}{d} \qquad \mathrm{Nu} = \frac{hd}{k} = \frac{a_k * k_a}{d}\frac{d}{k} = a_k. \tag{8}$$

Thus Nu can replace a_k so that

$$k_e = \mathrm{Nu} * k. \tag{9}$$

The bin door geometry in ZPPR is most like parallel plates closed at the top and bottom, but some air can escape through the upper doorjamb since it is not sealed at the top. The bottom is open so since the air between the door and the bin front is hotter than the surroundings, colder room air would come in the bottom to replace air lost out of the top.

Several investigators present data for heat transfer across an air space in the range of interest [8–11]. Yin's [9] experiments covered the complete Grashof number and aspect ratio range of interest in this work. Yin took data over the Grashof number range of 1.5×10^3 to 7.0×10^6 and covered the aspect ratio range of 4.9 to 78.7. The aspect ratio for the ZPPR doors is 23.3. The maximum calculated Grashof number in this problem is less than 7.0×10^6. In the low Grashof number range, ($< 10^3$) the Yin correlation yields values close to or less than 1 as it should since the heat transfer should be by conduction only. The Yin correlation, (10), covers the range of interest and has been used in the analysis where any values below 1 are replaced by 1 since that is the minimum value Nu can have. Consider the following:

$$\begin{aligned}\frac{hd}{k} &= 0.119 * \left\{\frac{g\rho^2 d^3 \beta (T_h - T_c)}{\mu^2}\right\}^{0.269} * \left\{\frac{d}{L}\right\}^{0.131} \\ &= 0.119 * \left\{\frac{g\rho^2 d^3 \beta \left(T_h - T_c\right)}{\mu^2}\right\}^{0.269} * \left\{\frac{1}{A_r}\right\}^{0.131},\end{aligned} \tag{10}$$

where g = acceleration due to gravity, d = distance between vertical plates, T_c = cold wall temperature, T_h = hot wall temperature, β = thermal expansion coefficient of air = $1/T_m$, for example, 1/300°K = 0.00333/°K, μ = dynamic viscosity of air, ρ = density of air, C_p = specific heat at constant density, and k = thermal conductivity. All properties are those of air evaluated at $T_m = (T_h + T_c)/2$. The first term in parentheses is the Grashof number based on the distance between the vertical walls. This correlation contains the aspect ratio, $A_r = L/d$, and shows that the Nusselt number decreases as the aspect ratio increases. For a constant distance between plates, the heat transfer decreases with height of door. The Yin correlation for $A_r = 1$ is used in all the calculations which is higher than for the ZPPR door A_r of 23.3. This higher value attempts to take into account the additional heat transfer due to flow through the door space. An estimate of the Nusselt number between the bin and the bin door assuming T_h = 140°C and T_c = 40°C and $d = 3 \times 2.54$ cm is Nu = 11.53.

The heat transfer between the fuel plates is estimated by a rectangular enclosure using a width of the distance between elements (0.25 inches) and the height of the element (2 inches). The Grashof number based on this distance is small enough that Nu = 1.

The space between the cavity door and the clamshell with a T_h = 210°C and T_c = 130°C with a distance, between them, of d = 0.35 inches (0.889 cm) yields a Gr = 1,384 and a Nusselt number of 1.47. A Nusselt number of 1 is used in the calculation for this region.

The vertical distance from the top of the fuel to the ceiling of the clamshell is 0.25 inches. Using Yin's correlation with Ar = 1 and the above temperatures and d gives Gr = 108, which is in the conduction region, so Nu of 1.00 is used. Horizontal surfaces give lower heat transfer than vertical surfaces do, so assuming conduction only, heat transfer in this region is a good assumption.

For the space above the clamshell, Grashof number is calculated with T_h = 112°C and T_c = 80°C and d = 0.875 in (2.22 cm) to obtain Gr = 2.15×10^4 and using the Yin correlation to calculate Nusselt number Nud = 3.07. Horizontal data would be lower, so a value of three is used in this region.

Jacob and Hawkins [12] P. 128 present a Nusselt number free standing wall correlation which was used to estimate an h for the outside of the bin door:

$$\mathrm{Nu} = 0.13\mathrm{Ra}^{1/3}. \tag{11}$$

The Rayleigh number, Ra, as originally derived by Bachelor [13] is a product of the Grashof number and the Prandtl number, Pr. The Rayleigh number, Ra, is defined as

$$\mathrm{Ra} = \mathrm{Gr} * \mathrm{Pr}, \qquad \mathrm{Gr} = \frac{g\rho^2 d^3 \beta \left(T_h - T_c\right)}{\mu^2}, \qquad \mathrm{Pr} = \frac{C_P \mu}{k}. \tag{12}$$

For air, the Prandtl number is about 0.7 so that, for air, the Rayleigh and Grashof numbers differ only by 30%. In this study, the Nusselt numbers represent the heat transfer of a vertical plate. Both the Nusselt numbers and the Rayleigh numbers in this correlation are based on the length, d, of the vertical plates.

For the bin door temperature of $T_h = 40$ and storage room of $T_c = 35$, $\mathrm{Ra} = 2.58 \times 10^9$. Equation (11) yields a Nusselt number of $\mathrm{Nu} = 178$. Using this Nu, the thermal conductivity of air of 0.012 W/m^2 °K and 70-inch wall, $h = 15,844$ W/m^2 °K. A value of 100 W/m^2 °K was used in all the calculations. The calculated temperatures would be a bit lower if the 15,844 W/m^2 °K was used, but not much.

4.3. Thermal Radiation. The thermal radiation model assumes that the radiation occurs between surfaces that are close together and parallel to each other. This implies that the radiation occurs mainly between surfaces that are parallel and opposite to each other so that the view factor between these surfaces is equal to one and equal to zero for other surfaces. Although this is an approximation, energy is still conserved [14]. This assumption causes the higher temperatures (i.e., fuel) to be higher than they would be if view factors to other surfaces were taken into account.

The model used for determining radiation between two parallel surfaces is shown in Figure 18 which considers a solid "a" with a surface "I" receiving radiation from solid "c" with surface "j" through an intervening transparent convecting medium "b."

At interface i, the solid medium, a, assumed to be at the lower temperature, interface i, receives heat by conduction and convection from the intervening medium, b, as well as radiation from the surfaces j which is at a higher temperature than surface i. Consider the following:

$$\text{at interface } i \quad k_a \frac{dT_a}{dx_{a_i}} = k_b \frac{dT_b}{dx_{b_i}} + \epsilon\sigma\left(T_j^4 - T_{iI}^4\right). \tag{13}$$

The higher temperature solid, c, loses heat by conduction and convection to the intervening medium and by radiation to surface i at a lower temperature. Consider the following:

$$\text{at interface } j \quad k_c \frac{dT_c}{dx_{c_j}} = k_b \frac{dT_b}{dx_{b_j}} + \epsilon\sigma\left(T_j^4 - T_i^4\right). \tag{14}$$

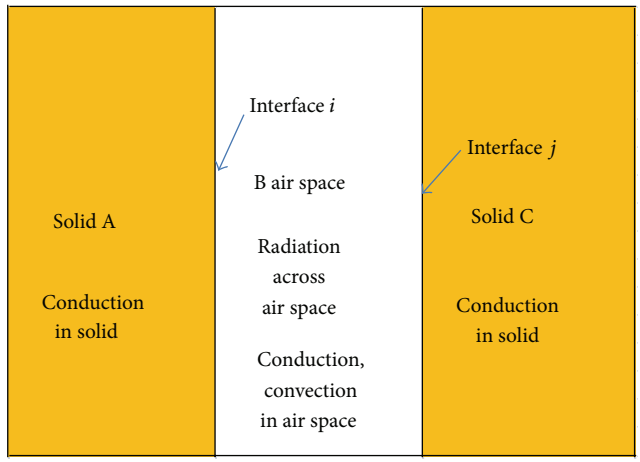

Figure 18: Geometry for the radiation model.

The radiation term is rearranged as

$$\left(T_j^4 - T_i^4\right) = C_{ij}\left(T_j - T_i\right), \tag{15}$$

where $C_{ij} \equiv (T_j + T_i)(T_j^2 + T_i^2)$.

In the finite difference solution, the C_{ij} is evaluated at the old time which causes these terms to be linear. Since the interior nodes are solved for explicitly, the only unknowns in the finite difference form of these two equations are the two interface temperatures, T_i and T_j. Therefore the above equations in finite difference form are two linear equations with two unknowns which are solved for the two surface temperatures. The solution for these interface temperatures replaces the interface boundary condition mentioned in Section 4.1 at all interfaces where thermal radiation is accounted for.

4.4. Effective Thermal Conductivities in the Concrete, Steel Sleeves, and Doors. The thermal conductivities in the steel regions and the concrete regions are modified to take into account some three-dimension heat losses. Increasing the thermal conductivity is equivalent to increasing the area of heat transfer. Although the transient behavior is affected by increasing the thermal conductivity, the steady state depends only on the thermal conductivity and not on the density or specific heat. The main interest here is the steady state, and the only transient of interest is the loss of storage cell cooling.

The length of the fuel element is 6.0 inches. The outside width of the fuel cavity liner is 8 inches. There is approximately 4 inches of concrete above, below, and to the sides of the 4-inch× 8-inch fuel storage cavity which results in a rectangle of 16 inches wide and 12 inches high. Using the midpoint of the 2-inch fuel to separate the higher from the lower portion of the area gives a distance of 7 inches to the top of the rectangle and 5 inches to the bottom. The upper concrete area for the 3D model heat loss is the 8×4 area above the sleeve and the two 7×4-inch areas on the side of the sleeve. The loss area for the 2D model is just the 6×4-inch area above the sleeve. Similarly, the lower concrete area for the 3D model heat loss is the 8×4 area below the sleeve and the two 5×4-inch

areas on the side of the sleeve. The loss area for the 2D model is just the 6 × 4-inch area below the sleeve. Therefore the heat transfer loss area ratios for the concrete are approximately as follows.

The ratio for the upper concrete is

$$k_{\mathrm{UC}} = \frac{(8+7+7)*4}{6*4} = 3.66. \quad (16)$$

The ratio for the lower concrete is

$$k_{\mathrm{LC}} = \frac{(8+5+5)*4}{6*4} = 3. \quad (17)$$

Similar reasoning for the steel sleeve gives the following ratios.

The ratio for the upper steel is

$$k_{\mathrm{US}} = \frac{(8+3+3)*0.188}{6*0.188} = 2.33. \quad (18)$$

The ratio for the lower steel is

$$k_{\mathrm{LS}} = \frac{(8+1+1)*0.188}{6*0.188} = 1.66. \quad (19)$$

Since the thermal conductivity of the steel is so high, the corrections to the steel do not make much difference in the answer.

5. Comparison to Data

Temperature measurements were made of the outside bin door, the storage sleeve door, and the clamshell in the ZPPR fuel storage cell in three locations. By comparing these measurements to the calculated temperatures, an estimate of the conservatism in the calculations of fuel element temperatures can be made. The fuel temperatures cannot be measured directly due to contamination and fuel preservation concerns which make it impractical to insert thermocouples into the clamshells while they are in storage. In order to measure the temperature of the fuel, it is necessary to open the bin doors, then open the cavity doors, then remove the clamshell, and bring it into the examination room. Then the bolts closing the clamshell can be removed and the clamshell is opened to expose the fuel, and then an optical pyrometer could be used to measure the fuel temperature. Significant heat loss would occur during this process in this new environment which would lower the maximum temperature of the fuel. The measured temperature would not represent the maximum temperature of the fuel in storage.

The conservatism in the model is contained mainly with the heat transfer through the air spaces where Nusselt numbers must be estimated and are used to represent the increase in conductive heat transfer due to free convection and the contact heat transfer resistances. The thermophysical properties of the solids are believed to be fairly accurate, although the emissivity of the surfaces is also an estimate based on experience. The emissivity of the fuel cladding is estimated on the low side as another conservative factor.

The measurements were made with an optical pyrometer. Measurements were made of the outside bin door, the inside cavity door, and the clamshell temperature. It is recognized that the cavity door temperature will decrease slowly after the bin door is opened, and the clamshell temperature will decrease slowly when the cavity door is open. Therefore, the cavity door temperature was measured quickly after the bin door was opened. Then the cavity door was opened, and the clamshell temperature was measured quickly.

Measurements were made at three different storage locations. Location 1 contains sixteen 5-inch Vendor 75 plates, and the other two locations have fifteen 6-inch Vendor 75 plates. The decay heats used in the computer base case computer run were based on sixteen 6-inch fuel elements with a total heat generation of 23.08 W calculated using the 1977 composition. The heat generation calculated for fuel where the Pu-241 has all decayed to Am-241 is 36.8 W. Comparisons here were made to the calculated base case of 16 fuel elements with 23.08 W. (Fifteen 6-inch fuel plates generate 21.6 W at the 1977 assumed fuel concentrations.) There is uncertainty about the heat generation in this fuel. It could be lower or higher than assumed in the model. The measurements were taken in a row of storage bins which were not backed against a symmetric set of bins but were backed against a concrete wall so that there was heat loss out the back of the bin rather than an adiabatic condition as assumed in the model. The particular bin was located between two other bins. The storage tubes were part of the middle four in the vertical alignment of six tubes so there were tubes above and below the measured tubes. The storage tubes on the sides and top/bottom contained clamshell with similar fuel to the ones measured so that the reflective heat transfer boundary conditions for the sides and top/bottom assumed in the model were reasonably represented. The loss of the adiabatic condition on the back of the storage bin might be represented by the difference shown in Table 5 for cases 1 and 4 which might result in 20°C lower maximum fuel, clamshell, and bin door temperatures. Since the maximum calculated temperatures are so much lower than the damage limit, this 20°C error would not affect the nondamage conclusion of this paper. In spite of these uncertainties, a comparison has been made.

The measurements made at the latter two locations are the closest to the base Case A modeled in the calculations. These are shown in Table 6 with approximate distances and temperatures. Also included are the analytical results for the base Case A and two additional cases (Cases B and C listed in Table 3) which model more realistic contact resistances.

Note that the differences between the temperatures of locations 2 and 3 are used as an estimate of the error (listed in Table 6) in the measurement and it is due primarily to the abovementioned uncertainties rather than the error of the optical pyrometer (0.2°C).

Figure 19 shows the comparison between the data (location 2) and the best model cases of Section 3.1. Note that three measured temperatures are shown, the bin door (black), the cavity door (green), and the clamshell (red). Case A calculated results, with the high contact resistances, are much higher than the data. Cases B and C temperatures do agree reasonably well with measured because the clamshell-sleeve and the sleeve-concrete interfaces contact resistances are set

Table 6: Measured and calculated temperatures at 3 locations.

	Distance from bin door front	Location 2	Location 3	Estimated error	Case A	Case B	Case C
Units	cm			Temperature ˚C			
Bin door	0	46.9	45.8	1.1	38.7	38.7	38.7
Cavity door	9	63.3	58.3	5.0	74.8	68.6	68.1
Clamshell	10	73.3	70.0	5.0	106.6	77.1	75.9

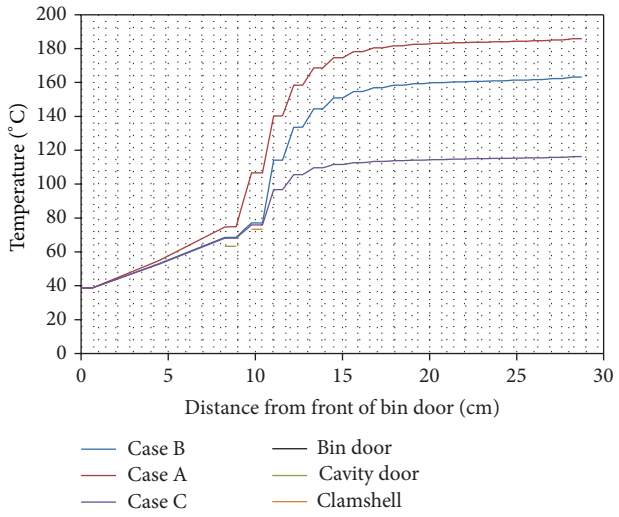

Figure 19: Comparison of measured temperatures to best model results.

to more realistic values. These are the same for Cases B and C. The fuel temperatures of Cases B and C are significantly different because the fuel contact resistance for Case B is high (the same as Case A) and is low for Case C. In the authors' estimation, this process of obtaining agreement with the measured data in Cases B and C and using high and low contact resistances, respectively, in Cases B and C implies that the fuel temperatures are bracketed by the temperatures of Cases B and C and are thus below the highest temperature in Case B of 164˚C.

Figure 19 gives somewhat of a false impression of the importance of the clamshell temperature since it appears only as a single point on the graph. This is because this is a temperature profile through the horizontal center of the clamshell. In reality, the clamshell completely surrounds the fuel and is 0.5 inches above the top of the fuel and in contact with that on the bottom. The clamshell has a high conductivity so that it is a good indicator of the fuel temperature. For example, it is seen that, in Case A, the fuel temperature is 20˚C higher than Case B and this causes the clamshell temperature to increase 20˚C as well. In Case 7 in Table 5 where thermal radiation has been neglected, the fuel maximum fuel temperature increases to 530˚C but the clamshell temperature increases to 186˚C. If the fuel temperature was really 530˚C, the clamshell temperature would have to be much higher than the measured value of 73˚C. So the conclusion is drawn that, with the measured clamshell temperatures being as low as they are, the fuel temperature cannot be above that calculated in Case A.

As a side note, the calculated bin door temperature is lower than the measurement indicating the estimated heat transfer coefficient to the storage room is too high. If this was decreased to obtain agreement, the other temperatures would increase.

There are two differences between the model and the clamshells measured which should be mentioned but do not change the above conclusions. The first is that the base case clamshell has one more fuel element than the clamshells at locations two and three since it has sixteen 6-inch fuel elements instead of 15. Modelling only 15 fuel elements instead of 16 would only lower the temperatures a small amount. The second is that the Pu-241 should have mostly decayed to Am-241 during the years of storage. This would increase the heat generation rate to 35 W rather than the 23 W assumed. The parameter study indicates the fuel temperature would be 60˚C higher with the higher heat generation (or 72˚C higher for the loss of cooling case). These temperatures are still far below the threshold of fuel damage.

6. Conclusions

Although there is uncertainty as to the heat generation rate in the measurements and uncertainty about how well the model matches the physical geometry, it is still evident that the calculations with high interface heat transfer resistances are higher than measurements in the locations measured. Although it has not been possible to measure the fuel temperatures in the clamshells, with the conservative assumptions being made, the authors expect that conservatively calculated fuel temperatures are significantly higher than actual temperatures. The maximum calculated fuel temperature with the most conservative assumptions (292˚C, (558˚F)) is significantly below the no-fuel failure criterion of 600˚C (1,112˚F). The main conclusion of this paper is that no damage has occurred due to the highly insulated characteristics of the ZPPR fuel storage facility. This conclusion is consistent with the measured data of the bin doors, the cavity doors, and the clamshell.

Due to the uncertainty in the temperature measurements locations, the heat generation rate, and the physical geometry of the cells measured, the following considerations are warranted. (1) The potential for high fuel element temperatures exists. These can occur in fully loaded clamshells. High fuel temperature can lead to problems. (2) The bin door enclosure represents a three-inch deep air resistance to heat transfer from the storage bin. (3) Measurement of the cavity door

temperature as soon as the bin door was opened and then measurement of the clamshell temperature as soon as the cavity door was opened have been made. These measurements have been used to calibrate the model temperatures of the fuel in the clamshell. (4) In order to verify the conclusion that no cladding damage has occurred from the high storage temperatures, some of the fuel should be inspected. The stored fuel where the storage temperatures are predicted to be the highest and have been stored at that temperature for a long time should be the ones checked for damage. If the fuel remains at high temperatures for a long time, it is possible that some cladding degradation would take place. Although the environment of the cell is probably low humidity, stress corrosion cracking is a possibility in the cladding.

These calculated results have been calibrated by measurement of the bin door, cavity door, and clamshell temperatures. The temperature measurements made show the analytical results are higher than the measurements and would be still higher if the higher heat generation corresponding to Pu-241 has decaying to Am-241 is used.

Disclaimer

This information was prepared as an account of work sponsored by an agency of the US Government. Neither the US Government nor any agency thereof, nor any of their employees, makes any warranty, expressed or implied, or assumes any legal liability or responsibility for the accuracy, completeness, or usefulness of any information, apparatus, product, or process disclosed, or represents that is use would not infringe privately owned rights. References herein to any specific commercial product, process, or service by trade name, trademark, manufacturer, or otherwise, do not necessarily constitute or imply its endorsement, recommendation, or favoring by the US Government or any agency thereof. The views and opinions of authors expressed herein do not necessarily state or reflect those of the US Government or any agency thereof.

Conflict of Interests

The authors declare that there is no conflict of interests regarding the publication of this paper.

Acknowledgment

This work is supported by the US Department of Energy, Office of Nuclear Energy, under DOE Idaho Operations Office Contract DE-AC07-05ID14517. Accordingly, the US Government retains a nonexclusive, royalty-free license to publish or reproduce the published form of this contribution, or allow others to do so, for US Government purposes.

References

[1] C. E. Till, Y. I. Chang, and W. H. Hannum, "The integral fast reactor-an overview," *Progress in Nuclear Energy*, vol. 31, no. 1-2, pp. 3–11, 1997.

[2] C. W. Solbrig, J. R. Krsul, and D. N. Olsen, "Pyrophorocity of uranium in long term storage environments," in *Proceedings of DOE Spent Nuclear Fuel: Challenges and Initiatives, ANS Topical Meeting*, Salt Lake City, Utah, USA, December 1994.

[3] N. Duckwitz, "Accident analysis for postulated releases from fuel handling and storage activities in the ZPPR complex," W7740 0283 ES, Argonne National Laboratory West, Rev. 0, 2004.

[4] R. T. Klann, B. D. Austin, S. E. Aumeier, and D. N. Olsen, "Inventory of Special Nuclear Material from the Zero Power Physics Reactor," Argonne National Laboratory West, 2001.

[5] T. Fukuoka and M. Nomura, "Evaluation of thermal contact resistance at the interface of dissimilar materials," *ASME Journal of Pressure Vessel Technology*, vol. 135, no. 2, Article ID 021403, 7 pages, 2013.

[6] A.-J. N. Khalifa, "Natural convective heat transfer coefficient: a review I. Isolated vertical and horizontal surfaces," *Energy Conversion and Management*, vol. 42, no. 4, pp. 491–504, 2001.

[7] A.-J. N. Khalifa, "Natural convective heat transfer coefficient—a review II. Surfaces in two- and three-dimensional enclosures," *Energy Conversion and Management*, vol. 42, no. 4, pp. 505–517, 2001.

[8] E. R. G. Eckert and W. O. Carlson, "Natural convection in an air layer enclosed between two vertical plates with different temperatures," *International Journal of Heat and Mass Transfer*, vol. 2, no. 1-2, pp. 106–120, 1961.

[9] S. H. Yin, T. Y. Wung, and K. Chen, "Natural convection in an air layer enclosed within rectangular cavities," *International Journal of Heat and Mass Transfer*, vol. 21, no. 3, pp. 307–315, 1978.

[10] V. Sernas and E. I. Lee, "Heat transfer in air enclosures of aspect ratio less than one," *Journal of Heat Transfer*, vol. 103, no. 4, pp. 617–622, 1981.

[11] M. N. A. Said and A. C. Trupp, "Laminar free convection in vertical air filled cavities with mixed boundary conditions," *Chemical Engineering Communications*, vol. 5, no. 1–4, pp. 93–107, 1980.

[12] M. Jacob and G. A. Hawkins, *Elements of Heat Transfer*, John Wiley & Sons, New York, NY, USA, 1957.

[13] G. K. Bachelor, "Heat transfer by free convection across a closed cavity between vertical boundaries at different temperatures," *Quarterly of Applied Mathematics*, vol. 12, pp. 209–233, 1954.

[14] R. L. Clarksean and C. W. Solbrig, "Minimization of the effect of errors in approximate radiation view factors," *Nuclear Engineering and Design*, vol. 149, pp. 431–440, 1994.